Haloferax volcanii immersed liquid biofilms develop independently of known biofilm machineries and exhibit rapid honeycomb pattern formation

Heather Schiller[1†], Stefan Schulze[1†], Zuha Mutan[1], Charlotte de Vaulx[1], Catalina Runcie[1], Jessica Schwartz[1], Theopi Rados[2], Alexandre W. Bisson Filho[2], and Mechthild Pohlschroder[1*]

[1]University of Pennsylvania, Department of Biology, Leidy Laboratories, Philadelphia, USA
[2]Department of Biology, Rosenstiel Basic Medical Science Research Center, Brandeis University, Waltham, Massachusetts, USA
[*]Correspondence should be addressed to: Mechthild Pohlschroder, pohlschr@sas.upenn.edu
[†]These authors contributed equally to the work

Abstract
The ability to form biofilms is shared by many microorganisms, including archaea. Cells in a biofilm are encased in extracellular polymeric substances that typically include polysaccharides, proteins, and extracellular DNA, conferring protection while providing a structure that allows for optimal nutrient flow. In many bacteria, flagella and evolutionarily conserved type IV pili are required for the formation of biofilms on solid surfaces or floating at the air-liquid interface of liquid media. Similarly, in many archaea it has been demonstrated that type IV pili and, in a subset of these species, archaella are required for biofilm formation on solid surfaces. In the model archaeon *Haloferax volcanii*, chemotaxis and AglB-dependent glycosylation also play a role in this process. *H. volcanii* also forms immersed biofilms in liquid cultures poured into Petri dishes. This study reveals that mutants of this haloarchaeon that interfere with the biosynthesis of type IV pili or archaella, as well as chemotaxis transposon and *aglB*-deletion mutants, lack obvious defects in biofilms formed in liquid cultures. Strikingly, we have observed that these liquid-based biofilms are capable of rearrangement into honeycomb-like patterns that rapidly form upon removal of the Petri-dish lid and are not dependent on changes in light, oxygen, or humidity. Taken together, this study demonstrates that *H. volcanii* requires novel, as yet unidentified strategies for immersed liquid biofilm formation and also exhibits rapid structural rearrangements, providing the first evidence for a potential role for volatile signaling in *H. volcanii*.

Importance
This first molecular biological study of archaeal immersed liquid biofilms advances our basic biology understanding of the model archaeon *Haloferax volcanii*. Data gleaned from this study also provide an invaluable foundation for future studies to uncover components required for immersed liquid biofilms in this haloarchaeon and also potentially for liquid biofilm formation in general, which is poorly understood compared to the formation of biofilms on surfaces. Moreover, the discovery of honeycomb pattern formation is likely to yield novel insights into the underlying interactions between the exopolysaccharide structure and cell arrangements within these biofilms and uncover mechanisms of cell-cell communication, a highly understudied topic in archaea.

Introduction

Prokaryotes have evolved a variety of strategies to mitigate the effects of environmental stress, including the establishment of biofilms, which are complex microbial communities surrounded by a matrix of extracellular polymeric substances (EPS). Of the bacteria and archaea found above the subsurface, an estimated 80% in soil and upper oceanic sediment exist in biofilms (1). It has been suggested that life within a biofilm may be the primary way of active life for both bacterial and archaeal species (1), with other bacterial-specific studies suggesting that life in a biofilm may be the default, with planktonic cells merely serving as mediators for the transition from one biofilm to the next (2). The advantages of being within a biofilm for bacterial cells range from communication and environmental stress protection to improved nutrient acquisition (3). Similarly, for archaeal species, the demonstrated advantages of biofilm living include conferring environmental stress protection, horizontal gene transfer, and syntrophy facilitation (4) as well as mechanical and structural stability provided by EPS (5, 6).

While some biofilms, such as those that play roles in wastewater treatment or bioremediation (7, 8) can provide a variety of important benefits to humans, others can cause serious harm, such as debilitating chronic infections (9–11), as biofilms confer reduced antibiotic and antimicrobial sensitivity (12, 13) that can render the embedded bacterial cells up to 1000 times less susceptible to treatments relative to planktonic cells (14). Thus, understanding biofilm formation is of significant public health interest.

To successfully form and sustain a biofilm, the cells within must be able to communicate with each other. Much of this bacterial cell-cell communication within the biofilm is performed via quorum sensing, whereby the concentration of secreted autoinducers, such as homoserine lactone (HSL), can signal the local density of cells (15, 16). Quorum sensing pathways have been shown to be required for proper biofilm formation in many species. For example, mutants of the bacterium

Pseudomonas aeruginosa lacking functional quorum sensing pathways have defects in the process of biofilm differentiation on surfaces (17). Moreover, *P. aeruginosa* cells unable to produce HSLs have an altered biofilm architecture, suggesting that HSLs regulate some aspects of biofilm structural development (18). Signaling between cells within a biofilm can also support biofilm heterogeneity, a key feature of biofilms that can contribute to increased antibiotic tolerance and pathogenicity (15, 19). Quorum sensing has also been shown to control mature biofilm formation through the regulation of EPS biosynthesis gene expression in *Vibrio cholerae* (20). Quorum sensing in archaea, while much less studied and not well-characterized, is likely to also play a role in archaeal biofilms (21).

A variety of proteins necessary for biofilm formation have been identified in an array of bacterial species. Biofilm formation requires type IV pili in organisms such as *P. aeruginosa* and *V. cholerae* (22–27). Flagella are also sometimes required for biofilms, such as those of *E. coli* and *P. aeruginosa* under certain conditions (24, 25, 28, 29). Additionally, in *P. fluorescens*, various surface adhesins are often critical to this process (30–32). While biofilms forming at surfaces have been extensively studied, much less is known about biofilms that form in liquid media. *Bacillus subtilis* and *P. aeruginosa*, for example, form pellicles — a type of biofilm that floats at the air-liquid interface of a culture — and flagella-based motility is important for successful pellicle formation in both organisms (33–35). Chemotaxis and oxygen sensing have also been shown to play crucial roles in the formation of pellicles in *B. subtilis* (35).

Archaea also readily form biofilms in a variety of habitats (4). The genetically tractable cren- and euryarchaeal species tested thus far form surface-attached biofilms in a type IV pilus-dependent manner, and, in a subset of these species (such as *Sulfolobus acidocaldarius* and *Methanococcus maripaludis*), biofilm formation is also dependent on the archaella — structures analogous to the bacterial flagella — under certain conditions (4, 36, 37). The model haloarchaeon *Haloferax volcanii* can form biofilms on surfaces at the air-liquid interface (ALI) of a culture in a type IV pili-dependent but archaella-independent manner (38). Strains lacking the genes encoding the adhesion pilins, the prepilin peptidase, or components of the pilus biosynthesis pathway (Δ*pilA1-6*, Δ*pibD,* and Δ*pilB1/C1* or Δ*pilB3C3*, respectively) are impaired in adhesion to coverslips at the ALI (36, 38–41). While biofilm formation in *H. volcanii* presumably also requires the chemotaxis machinery, as a transposon insertion between the *cheB* and *cheW1* genes results in a mutant having an adhesion defect, *H. volcanii* biofilm formation is not impaired in a non-motile mutant lacking the archaellins *arlA1* and *arlA2* (38, 42).

Archaea can also be found in floating liquid biofilms (43, 44). Moreover, Chimileski et al. recently described *H. volcanii* immersed liquid biofilms that form in static-liquid cultures (45). These biofilms contain polysaccharide, based on Concanavalin A staining, and eDNA, based on DAPI staining, as major structural components, and possibly also include amyloid proteins based on Congo Red and Thioflavin T staining (45). Chimileski et al. also reported that after homogenization of the immersed liquid biofilm, aggregation occurred in as little as three hours, and the biofilm became more concentrated and denser over the course of 48 hours (45). However, the molecular mechanisms required for the formation of these biofilms is not yet known.

Here we report that *H. volcanii* immersed liquid biofilms form independently of type IV pili along with chemotaxis and archaella machineries, demonstrating that the mechanisms required for the formation of *H. volcanii* immersed liquid biofilms differ significantly from those required for the formation of an archaeal biofilm on an abiotic surface. We have also discovered a unique, rapid change in the macroscopic, three-dimensional organization of the biofilm, forming a honeycomb-like pattern in response to disturbance of the headspace caused by the removal of the lid of the Petri dish containing the immersed liquid biofilm cultures. Moreover, a volatile factor released into the headspace by the immersed liquid biofilm may affect the structural relationship between cells such that rapid removal of that factor results in the dramatic appearance of honeycomb-like structures formed by cells within the immersed liquid biofilm.

Materials and Methods

Strains and growth conditions. *H. volcanii* wild-type strain H53 and its derivatives (Table 1) were grown aerobically at 45˚C in liquid (orbital shaker at 250 rpm) or on solid semi-defined Hv-Cab medium (46). H53, Δ*pibD*, Δ*pilA1-6*, Δ*pilB1C1*, Δ*pilB3C3*, Δ*pilB1C1B3C3*, Δ*arlA1*, Δ*arlA2*, Δ*arlA1-2*, Δ*aglB*, and Δ*agl15* media were additionally supplemented with tryptophan and uracil (both at 50 µg · ml^{-1} final concentration); *cheB-cheW1::tn*, *cheF::tn*, Δ*pssA*, and Δ*pssD* media were supplemented with uracil (50 µg · ml^{-1} final concentration); H98 and Δ*cetZ1* media were supplemented with thymidine and hypoxanthine (both at 40 µg · ml^{-1} final concentration) as well as uracil (50 µg · ml^{-1} final concentration) (47). Solid media plates contained 1.5% (wt/vol) agar. *Haloferax mediterranei* was grown aerobically at 45˚C in Hv-Cab medium (46).

Table 1: Strains used in this study.

Strain	Genotype	Reference or Source
H53 (wild-type)	Δ*pyrE2* Δ*trpA*	(48)
MT4	H53Δ*pibD*	(38)
RE 43	H53Δ*pilA1-6*	(40)
GL 20	H53Δ*pilB1C1*	(41)
RE 26	H53Δ*pilB3C3*	(49)
GL 21	H53Δ*pilB1C1B3C3*	(41)
EY9	*cheB-cheW1::tn* Location: 1115464	(42)
EY31	*cheF::tn* Location: 1110849	(Unpublished)
MT14	H53Δ*arlA1*	(49)
MT30	H53Δ*arlA2*	(49)
MT2	H53Δ*arlA1-2*	(38)
Δ*aglB*	H53*HVO_1530::trp*	(50)
Δ*agl15*	H53Δ*HVO_2055::trp*	(51)
FH55	H53Δ*pssA*+pTA963	(52)
FH69	H53Δ*pssD*+pTA963	(52)
H98	Δ*pyrE2* Δ*hdrB*	(48)
ID59	H98Δ*cetZ1*	(53)

Immersed liquid biofilm formation. Biofilms of strains tested in this study were prepared and observed as follows: strains were inoculated in 5 mL of Hv-Cab medium followed by overnight incubation at 45°C with shaking (orbital shaker at 250 rpm) until the strains reached mid-log phase (OD_{600} 0.3-0.7). Mid-log cultures were diluted to an OD_{600} of 0.05 at a final volume of 20 mL followed by shaking incubation at 45°C for 48 hours. Cultures were poured into sterile Petri dishes (100mm x 15mm, Fisherbrand) after the 48-hour incubation period. Poured cultures were placed in plastic bins and incubated at 45°C without shaking for 18 ± 3 hours after which the resulting immersed liquid biofilms were observed and imaged.

Honeycomb pattern observation. After an incubation period of 18 ± 3 hours post-pouring with resulting immersed liquid biofilm formation, *H. volcanii* wild-type and mutant strain cultures were observed for honeycomb pattern formation. Without disturbing the biofilms, the lids of the Petri dishes were removed immediately after plastic bin lid removal and observations were made on the speed and formation of the honeycomb pattern along with its dispersal. Honeycomb pattern formation was recorded and/or imaged using an iPhone (Fig. 1, Fig. 4, Fig. S2, and Fig. S4), Canon EOS Digital Rebel XSi (Fig. 3), and Nikon D3500 DX-Format DSLR Two Lens (lens 18-55mm f/3.5-5.6G, video setting 60fps) (Fig. 2, Fig. S5, Movie S1, and Movie S2).

Quantification of immersed liquid biofilm coverage. Immersed liquid biofilm coverage within the Petri dish was quantified using Fiji (54) by converting the image to grayscale and binary, drawing a region of interest (ROI) around the Petri dish, and measuring the area corresponding to the biofilm as a percentage of the total ROI. Each strain was tested at least twice.

Kinetics of honeycomb pattern formation and dispersal. Calculation of when the immersed liquid biofilm began making honeycomb patterns was determined by measuring the time it took for honeycomb patterns to form after the lid of the Petri dish was removed. Time to peak honeycomb formation was defined as the point at which honeycombs were the clearest and covered the greatest extent of the plate after lid removal. The point of dispersal was defined as the time at which honeycombs moved substantially outward, distorting their initial configuration. Each strain was tested at least twice.

***H. volcanii* anaerobic growth curve.** To optimize Hv-Cab medium for anaerobic growth, we tested fumarate concentrations between 0 mM and 60 mM with 25 mM final concentration of PIPES buffer (adapted from (55)). Hv-Cab anaerobic medium used for anaerobic immersed liquid biofilm and honeycomb pattern formation experiments contained 45 mM sodium fumarate with 25 mM final concentration of PIPES buffer; uracil added to this medium was dissolved in ddH_2O (Millipore Sigma) (final concentration 2 μg/mL) rather than DMSO. Media was de-gassed in the microaerobic chamber 24 hours before use. *H. volcanii* liquid cultures were inoculated from colonies into 5 mL of each of the six fumarate Hv-Cab media followed by continuous shaking at 45˚C. Subsequently, each culture was transferred into wells of a 96-well plate and diluted to an OD_{600} of 0.01 (with the exception of the 0 mM fumarate medium, which was diluted to 0.005) with fresh liquid medium added to bring the final volume to 300 µL (16 technical replicates of one biological replicate). OD_{600} recordings were taken every 30 minutes for 44 hours and then every 60 minutes for 96 hours (6 days total) with an Epoch 2 Microplate Spectrophotometer (Biotek, Winooski, VT) within a rigid gloveless hypoxic chamber (Coy Lab, Grass Lake, MI). The plate underwent a double orbital shake for one minute before each measurement.

Immersed liquid biofilm and honeycomb pattern formation in anaerobic chamber. Strains were inoculated aerobically in 5 mL of 45 mM fumarate Hv-Cab medium followed by overnight aerobic incubation at 45°C with shaking (orbital shaker at 250 rpm) until the strains reached mid-log phase (OD_{600} 0.3-0.7). Mid-log cultures were diluted to an OD_{600} of 0.05 at a final volume of 20 mL followed by aerobic shaking incubation at 45°C for 48 hours. After the 48 hours incubation period, cultures were poured into sterile Petri dishes (100mm x 15mm, Fisherbrand) in an anaerobic chamber (Coy) with a Palladium catalyst; oxygen gas was purged and replaced with a gas mix of hydrogen/nitrogen (5%/95%). Poured cultures were left in the anaerobic chamber for 24 hours in an incubator (41˚C), after which the resulting immersed liquid biofilm and honeycomb pattern formation were observed and imaged. Note that for one of the plates that was tested, the oxygen level in the anaerobic chamber was between 7 and 13 ppm. Strains were left in the anaerobic chamber for an additional 18 hours either at room temperature or in an incubator (45˚C) and then observed again for both immersed liquid biofilm and honeycombs.

Dew Point Generator. Experiments were performed using the same protocol for immersed liquid biofilm formation with the exception that Petri dishes were not covered with Petri dish lids, and the Petri dishes were placed in plastic airtight containers connected to a Dew Point Generator (DPG) (LI-610 Portable Dew Point Generator, LI-COR) at room temperature. Air from the DPG entered the container through a silicone tube and exited the container through a silicone tube at the opposite end of the container. The airflow was dispensed at 18-20 cm^3/min at the appropriate temperature to confer the desired relative humidity level (calculated as described in the manual). For experiments shown in Fig. 4C and D, the inside of the airtight containers was lined with Styrofoam and aluminum foil to reduce the headspace of the Petri dish and therefore concentrate the distributed airflow. A hygrometer was also present inside the container to measure relative humidity levels, except for the experiment described in Fig. 4B.

Results

Development of a rapid immersed liquid biofilm formation assay

Chimileski et al. described the formation and maturation of static liquid biofilms from late-log phase (OD_{600} of 1) liquid shaking cultures after an incubation period of seven days (45). To further characterize immersed liquid biofilms and determine the *H. volcanii* proteins required for its formation, we set out to develop a fast and reproducible protocol for immersed liquid biofilm formation. Using a stationary phase liquid culture transferred from a shaking culture tube into a Petri dish, we observed that *H. volcanii* strain H53, the wild-type strain used in this study, begins forming an observable biofilm after as little as eight hours of static incubation, with a robust biofilm being formed within 15 hours and not changing significantly for the next six hours. Therefore, we chose to set our standard immersed liquid biofilm observation time at 18 ± 3 hours of static incubation (Fig. 1A).

While the timing of immersed liquid biofilm formation under the conditions tested was reproducible, they presented stochastic variations in shape, color intensity (likely based on differences in cell density), and coverage of the Petri dish (Fig. 1B). The shape of immersed liquid biofilms in this study ranged from dense, circular areas to diffuse, amorphous shapes. Coverage of the dish varied widely, with the coverage of the area ranging from 67% to 100% in 25 wild-type plates and an average coverage of 91% ± 10% (Fig. S1A).

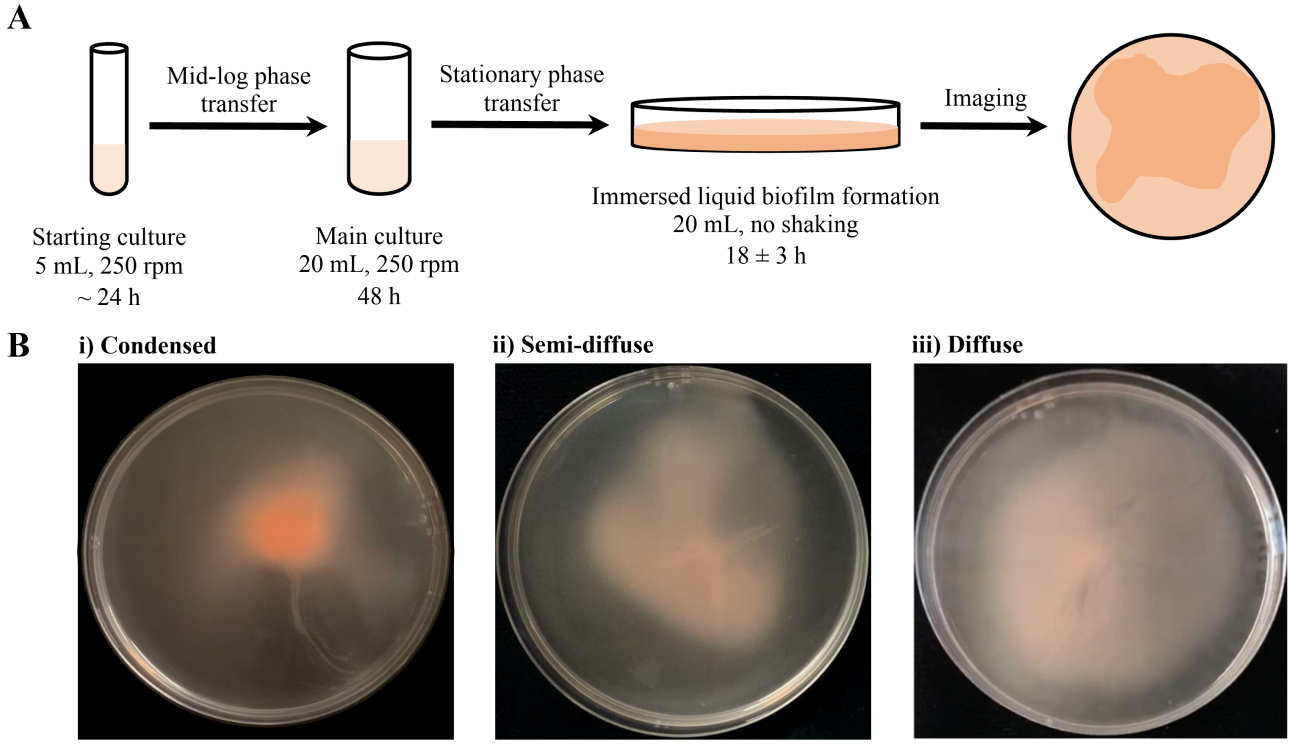

Figure 1: Optimized protocol for *H. volcanii* immersed liquid biofilm formation. (A) A schematic description of the protocol used for the reproducible observation of immersed liquid biofilm formation is shown. Single colonies are inoculated and incubated while shaking until they reach mid-log phase (OD_{600} between 0.3 and 0.7). Cultures are then diluted to an OD_{600} of 0.05, to ensure the same starting OD_{600} for different cultures, and incubated again on a shaker for 48 hours, at which point they are in stationary phase (OD_{600} of 1.8 or greater). The cultures are then poured into sterile plastic Petri dishes and statically incubated. Immersed liquid biofilm formation can be observed reproducibly after 18 ± 3 hours. All incubations were performed at 45°C. **(B)** Representative images for stochastic variations in the shape and color of immersed liquid biofilms for the wild-type are shown, ranging from dark, condensed (i) to light, diffuse immersed liquid biofilms (iii). All immersed liquid biofilms are imaged after 18 ± 3 hours of static incubation. The diameter of the Petri dishes is 10 cm.

Immersed liquid biofilm formation is independent of known *H. volcanii* components required for biofilm formation on surfaces at the air-liquid interface

Similar to many other archaea and bacteria, evolutionarily-conserved type IV pili are required for *H. volcanii* biofilm formation on surfaces at the air-liquid interface (38, 40). To determine whether type IV pili are also important for immersed liquid biofilm formation, we tested the Δ*pilA1-6* and Δ*pibD* strains, which encode the adhesion pilins and the prepilin peptidase, respectively, neither of which adhere to coverslips at the air-liquid interface of a liquid culture after 24 hours of incubation (36, 38, 39). Both the *H. volcanii* Δ*pibD* and Δ*pilA1-6* strains formed immersed liquid biofilms comparable to those of wild-type (Table 2 and Fig. S2A). The ability of cells lacking PibD to form these liquid biofilms is particularly notable, as it is responsible for processing all pilins in *H. volcanii* (56). Furthermore, consistent with these results, the Δ*pilB3C3* strain lacking the ATPase (PilB) and the transmembrane component (PilC), both of which are required for PilA1-6 pili assembly (40, 49), as well as the recently characterized Δ*pilB1C1* strain, which lacks PilB and PilC homologs that are likely involved in assembling pili composed of a distinct set of pilins and exhibits defective surface adhesion (41), also form immersed liquid biofilms similar to those of wild-type. A mutant strain lacking both *pilB* and *pilC* paralogs (Δ*pilB1C1B3C3*) can also form immersed liquid biofilms (Table 2 and Fig. S2A).

Since a screen of an *H. volcanii* transposon insertion library for motility or adhesion-defective *H. volcanii* mutants revealed two mutant strains having insertions in the intergenic regions between chemotaxis genes *cheB* (*hvo_1224*) and *cheW1* (*hvo_1225*) (42) and one mutant strain with a transposon insertion within *cheF* (*hvo_1221*) (data not shown) that have severe motility and adhesion defects, chemotaxis likely plays an important role in adhesion as a prerequisite to biofilm formation in *H. volcanii* . However, immersed liquid biofilm formation comparable to that of *H. volcanii* wild-type cultures was observed in the *cheB-cheW1::tn* as well as *cheF::tn* mutant strains (Table 2 and Fig. S2A).

As noted, *cheB-cheW1::tn* and *cheF::tn* are also non-motile, strongly suggesting that archaella – which are required for swimming motility, but, unlike in some other archaea, are not required for biofilm formation on surfaces in *H. volcanii* (38) – are also not involved in immersed liquid biofilm formation in *H. volcanii*. Three archaellin mutants, Δ*arlA1* (non-motile), Δ*arlA2* (hypermotile), and the double knockout Δ*arlA1-2* (non-motile), were able to form immersed liquid biofilms comparable to wild-type (Table 2 and Fig. S2A). Strains that lack AglB, the oligosaccharyltransferase involved in *N*-glycosylation of archaellins and type IV pilins more quickly forms microcolonies compared to wild-type in *H. volcanii* (57). However, neither the Δ*aglB* strain, nor a deletion strain lacking a gene encoding a key component of a second *N*-glycosylation pathway Agl15, conferred immersed liquid biofilm formation defects (Table 2 and Fig. S2A).

We also tested for immersed liquid biofilm formation in deletion mutants involved in lipid anchoring of archaeosortase (ArtA) substrates (52). We speculated that the proper anchoring of some of these ArtA substrates, which includes the S-layer glycoprotein, might potentially be required for immersed liquid biofilm formation. However, two proteins

critical for lipid anchoring of ArtA substrates (52), the phosphatidylserine synthase (PssA) and the phosphatidylserine decarboxylase (PssD), do not appear to be required for formation of these liquid biofilms, as the deletion strains, Δ*pssA* and Δ*pssD*, respectively, form immersed liquid biofilms similar to those of the wild-type. Finally, the ability to form rods did not appear to be important for immersed liquid biofilm formation, as the Δ*cetZ1* strain, which lacks the ability to form rods (53), formed these biofilms (Table 2 and Fig. S2A).

Similar to the wild-type strain, the mutant strains tested (as well as the Δ*cetZ1* parental strain H98) formed immersed liquid biofilms of varying shape and color, and the extent of Petri dish coverage did not differ substantially from the wild-type (Fig. S1A). Overall, these results indicate that key components of the machinery required for surface adhesion, microcolony formation, and swimming motility are not involved in immersed liquid biofilm formation.

Immersed liquid biofilms self-assemble into honeycomb patterns upon removal of Petri dish lid

While testing strains for their ability to form immersed liquid biofilms in Petri dishes, we discovered a novel and reproducible phenomenon: removing the lid of the Petri dish caused a rapid, but transient, macroscopic, three-dimensional change in the organization of the immersed liquid biofilm that resulted in the formation honeycomb-like structures (Fig. 2; Movie S1). After incubation at 45˚C for 18 ± 3 hours, removal of the Petri dish lid led to the emergence of a readily observable honeycomb pattern in the immersed liquid biofilm that started within 20 ± 4 seconds (range: 13 s to 27 s) after lid removal in the wild-type strain (Fig. S1B). However, when the immersed liquid biofilm was incubated at room temperature, the honeycomb pattern emerged more slowly, as the honeycomb patterns do not appear before two minutes from lid removal.

Table 2: Immersed liquid biofilm phenotypes of motility and adhesion mutants.

Strain	Motility	Surface Adhesion	Microcolony Formation	Immersed Liquid Biofilm Formation	References
H53	++	++	++	++	(38, 40)
Δ*pibD*	-	-	-	++	(38)
Δ*pilA1-6*	+	-	-	++	(40)
Δ*pilB1C1*	n.d.	+	+	++	(41)
Δ*pilB3C3*	++	+	+	++	(40, 41)
Δ*pilB1C1B3C3*	n.d.	+	+	++	(41)
cheB-cheW1::tn	-	+	n.d.	++	(42)
cheF::tn	-	+	n.d.	++	(Unpublished)
Δ*arlA1*	-	n.d.	n.d.	++	(49)
Δ*arlA2*	+++	n.d.	n.d.	++	(49)
Δ*arlA1-2*	-	++	n.d.	++	(38)
Δ*aglB*	-	++	++ / early	++	(57, 58)
Δ*agl15*	n.d.	n.d.	n.d.	++	
Δ*pssA*	+	n.d.	n.d.	++	(52)
Δ*pssD*	+	n.d.	n.d.	++	(52)
H98	++	++	++	++	(Unpublished)
Δ*cetZ1*	n.d.	n.d.	n.d.	++	

Phenotypes are described semi-quantitatively as no (yellow, "-"), reduced (light blue, "+"), wild-type like (blue, "++"), and increased (dark blue, "+++") motility, surface adhesion or microcolony formation. All tested strains exhibited wild-type like immersed liquid biofilm formation. References are given for motility, surface adhesion and microcolony formation phenotypes, while the ability to form immersed liquid biofilms is based on the results presented in this study.

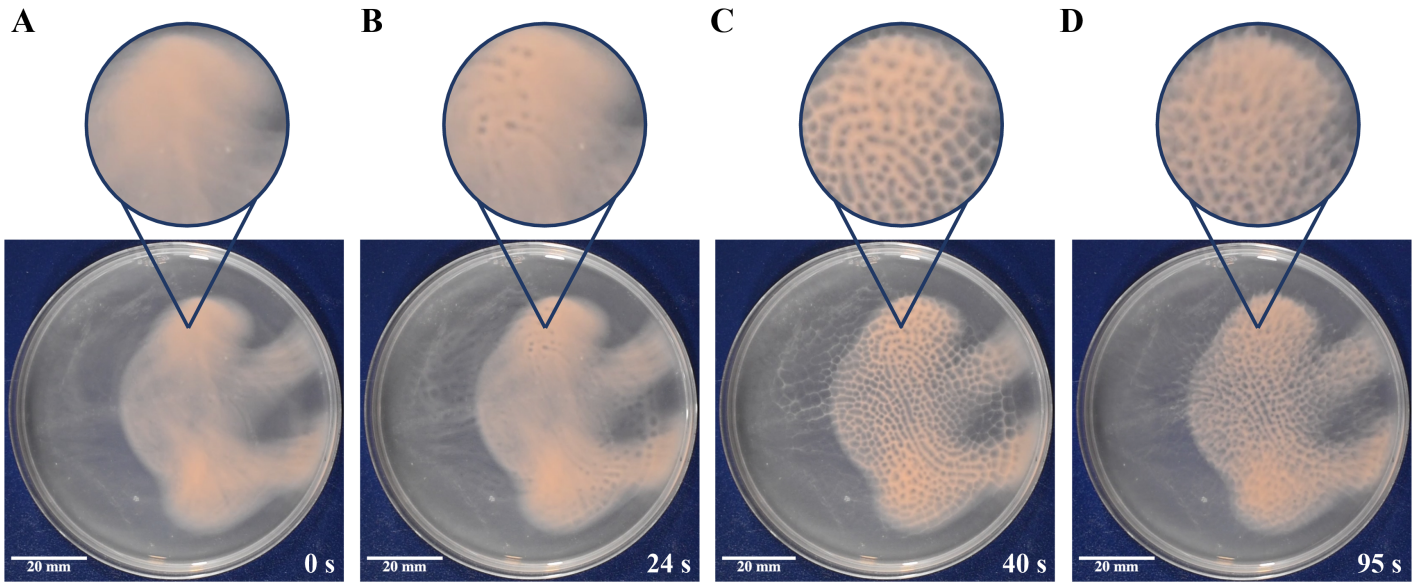

Figure 2: Immersed liquid biofilms exhibit honeycomb pattern formation. (A) Representative images of a wild-type immersed liquid biofilm immediately after Petri dish lid removal, followed by **(B)** start of honeycomb formation 24 seconds after lid removal, **(C)** peak honeycomb pattern formation 40 seconds after lid removal, and **(D)** dispersal of the honeycomb pattern 95 seconds after lid removal, are shown. Insets are digitally magnified images (2.0x) of the indicated area. The corresponding video can be viewed as Movie S1.

The pattern generally begins in one to two sections of the dish and quickly spreads to cover the biofilm until it reaches its peak formation (Fig. 2B); in wild-type, peak honeycomb formation occurred 38 ± 7 seconds (range: 25s to 55s) after lid removal (Fig. S1C). The honeycomb patterns are transient, as dissipation of the honeycombs begins 29 ± 9 seconds (range: 18s to 57s) after the peak of honeycomb pattern formation in wild-type (Fig. 2C; Fig. S1D). Interestingly, while the immersed liquid biofilms form close to the bottom of the Petri dish, the honeycomb-like structures extend further into the liquid and appear to dissipate close to the ALI (Movie S2). After honeycomb pattern formation and subsequent dissipation, placing the lid back onto the plate and allowing the immersed liquid biofilm to reform for at least one hour enables the pattern formation to again occur once the Petri dish lid is removed again. Honeycomb pattern formation is not dependent on light, as removing the lid in a dark room results in honeycombs as well (data not shown).

The formation of honeycomb patterns can be split into four distinct phases: pre-honeycomb pattern formation, which consists of the immersed liquid biofilm before honeycomb pattern formation begins (Fig. 2A), start of honeycomb pattern formation, when the first honeycombs appear (Fig. 2B), peak-honeycomb pattern formation, which is when the honeycomb pattern covers the greatest extent of the biofilm (Fig. 2C), and dispersal of honeycomb patterns, which occurs when the honeycomb pattern begins to dissipate and eventually returns to the settled biofilm state (Fig. 2D). Similar to our results showing that each mutant strain tested was able to form an immersed liquid biofilm, every mutant strain tested also formed honeycomb patterns (Fig. S2B) and honeycomb pattern formation followed a similar time frame compared to that of wild-type in all three phases (Fig. S1B, C, and D).

Honeycomb pattern formations occur under anaerobic conditions

To determine the factor(s) that induce the morphological change upon removal of the lid, we next sought to identify conditions under which honeycomb-like structures fail to develop. Having determined that honeycomb patterns were observed in Petri dishes as well as 6- and 24-well plates but not in standing tubes containing 5 mL liquid cultures (data not shown), we first investigated whether differences in oxygen concentrations play a role in honeycomb pattern formation. While *H. volcanii* is a facultative anaerobe, to the best of our knowledge, *H. volcanii* biofilm experiments had not previously been carried out under anaerobic conditions.

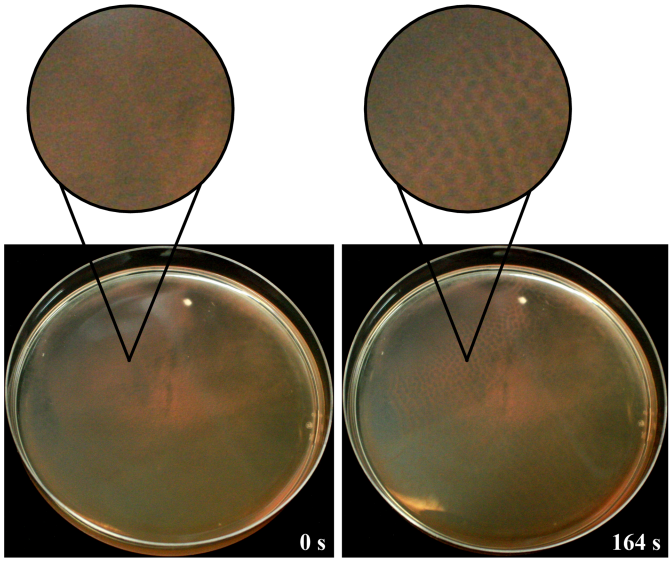

Figure 3: Honeycomb patterns form in the absence of oxygen. Removal of the Petri dish lid of a wild-type culture immersed liquid biofilm in anaerobic chamber results in the formation of honeycomb patterns. Representative images were taken immediately after opening the lid (left) and after 2 minutes and 44 seconds (right) at room temperature. Insets are digitally magnified images (2.9x) of the indicated area. Images shown are representative for two replicates tested. The Petri dish diameter is 10 cm.

Following a previous study (55), we modified the Hv-Cab medium to contain fumarate as an electron acceptor and PIPES as a buffer. We tested a range of fumarate concentrations along with 25 mM of PIPES buffer via an anaerobic growth curve using a 96-well plate assay (Fig. S3A). While fumarate was required for cell growth under anaerobic conditions, differences between the tested fumarate concentrations were negligible. Therefore, we chose the intermediate concentration of 45 mM fumarate for further experiments (Fig. S3B).

Using the fumarate Hv-Cab medium, we tested the ability of wild-type cells to form honeycomb patterns under anaerobic conditions. We used the same protocol as shown in Fig. 1A, with the exception that stationary phase liquid cultures were poured into, and incubated (at 41˚C) in, Petri dishes that were maintained in an anaerobic chamber. After 24 hours, immersed liquid biofilms were tested for their ability to form honeycomb patterns by opening the Petri dish lid inside the anaerobic chamber. Surprisingly, we determined that the formation of honeycomb patterns under anaerobic conditions was comparable to those observed in aerobic cultures (Fig. 3). The cultures were incubated for an additional 18 hours at either room temperature or at 45˚C in the anaerobic chamber, after which immersed liquid biofilms were re-established; honeycomb patterns formed upon removal of the lid at the same rates as they did in aerobic cultures at both of these temperatures (Fig. 3).

Headspace volatile substances may regulate honeycomb pattern formation

We suspected that volatile compounds that accumulate under the Petri dish lid might induce honeycomb pattern formation when suddenly released via removal of the Petri dish lid. However, we also considered the possibility that the induced formation of honeycomb patterns does not represent a biological response to a change in the environment but, for instance, results from changes in humidity levels of the air adjacent to the culture induced by the removal of the lid. This change could then theoretically lead to phase separation in the liquid culture, resulting in the formation of honeycomb-like structures.

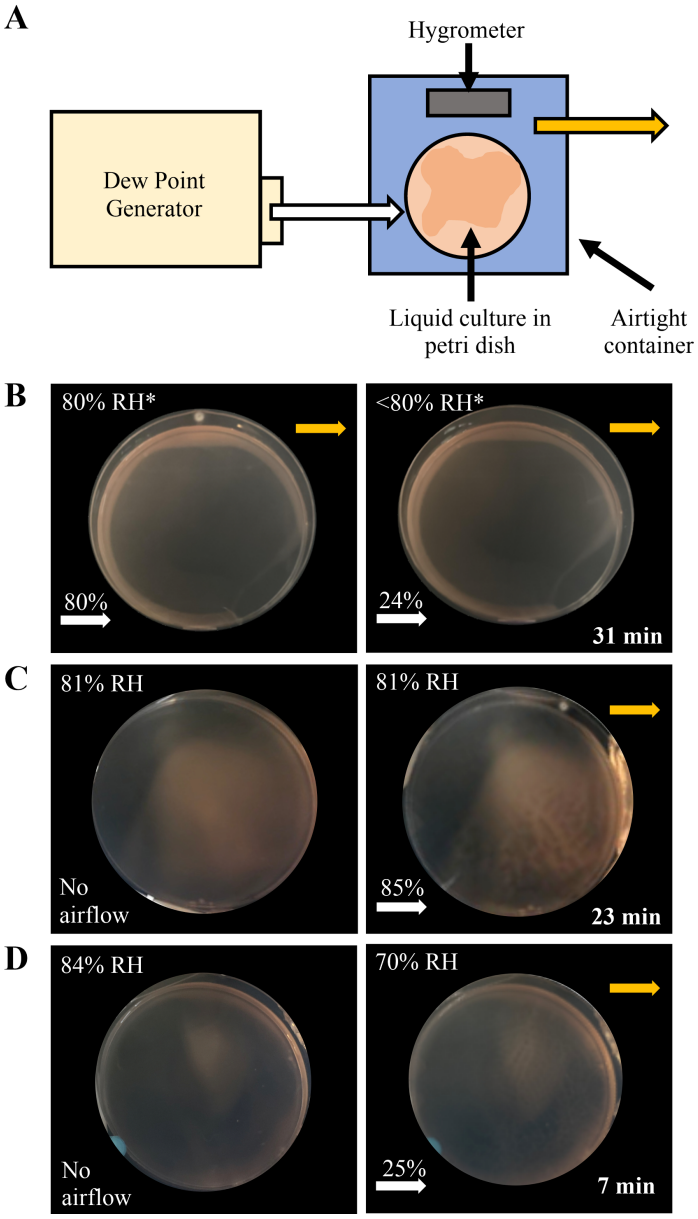

Figure 4: Volatile dissipation likely induces honeycomb pattern formation. (A) Schematic representation of the Dew Point Generator (DPG) setup. The DPG was attached to a small, airtight plastic bin with two tube attachments, an input airflow tube (white arrow) from the DPG and an output airflow tube (yellow arrow). The bin contained a lidless Petri dish with liquid culture and a hygrometer. The DPG was set at high- or low-humidity levels, depending on the experiment. **(B)** Immersed liquid biofilms were formed while a constant airflow over the Petri dish was provided through the DPG (left). The humidity level was then changed from 80% to 24% RH (right), which did not trigger honeycomb pattern formation. **(C)** Immersed liquid biofilms were formed without any airflow (DPG not connected to the bin, left). After connecting the DPG with high-humidity (85% RH) airflow to the bin, honeycomb pattern formation was observed (right). **(D)** After immersed liquid biofilms were formed at no airflow, low-humidity (25% RH) airflow triggered the formation of honeycomb patterns (right). In (B), (C), and (D), the leftmost images were taken at the beginning of the experiments, and the rightmost images were taken at the indicated time points in the bottom right corner. White arrows indicate the entry point of the airflow from the DPG with the above percentage indicating the RH of the input airflow. Yellow arrows indicate the airflow exit point. Percentages in the top left corner indicate the relative humidity in the box as measured on the hygrometer. Experiments in (B), (C), and (D) are representative of one, five, and four biological replicates, respectively. The diameter of the Petri dishes is 10 cm. *, RH level is an estimate; no hygrometer present.

To distinguish between these two hypotheses – volatile dissipation-dependent honeycomb pattern formation versus humidity-dependent honeycomb pattern formation – we used a Dew Point Generator (DPG), which dispenses air at controlled humidity levels (Fig. 4A). We attached airtight containers, each containing a liquid culture in a Petri dish lacking a lid, as well as a hygrometer to measure relative humidity levels, to the DPG. In the first experiment, we poured the liquid culture into the Petri dish and attached the DPG output tubing to the container, but did not turn on the airflow. After 16.5 hours post-pouring, an immersed liquid biofilm had formed and we turned on the airflow. This initial airflow represents conditions that are similar to the opening of the Petri dish lid in experiments without the DPG, since the DPG required a brief warm-up period before the airflow reached the set point of 80% relative humidity (RH). Consequently, as expected, the lower-humidity initial airflow triggered the formation of honeycomb patterns. Once the DPG airflow reached 80% RH, we let the immersed liquid biofilm re-equilibrate under constant 80% RH airflow for six hours. We then lowered the humidity level of the airflow to 24% RH while maintaining the same air flow rate. We maintained the 24% RH airflow for 2.5 hours, and during that time no honeycomb pattern formation was observed (Fig. 4B). These results suggest that the change in humidity does not trigger the formation of honeycombs, as maintaining a constant airflow while lowering the humidity of the airflow does not trigger honeycomb pattern formation.

We also noted that immersed liquid biofilms formed despite the presence of constant airflow, preventing the accumulation of volatiles or depletion of oxygen in the air surrounding the liquid culture. This observation was confirmed for cultures incubated with 80-85% RH airflow overnight, for which the immersed liquid biofilms tended to form along the edges of the Petri dish, as can be seen in Fig. S4A. Nevertheless, immersed liquid biofilms present at the center of the dish were observed as well (Fig. S4B).

Since humidity did not appear to be the factor triggering honeycomb pattern formation, we hypothesized that honeycomb-patterns are induced by the dissipation of an accumulated compound in the headspace. We predicted that going from either no airflow to 85% RH airflow or from no airflow to 25% RH airflow would prompt the formation of honeycomb patterns. Since the RH inside the container was 80% or higher when no airflow was applied, an 85% RH airflow was comparable to the humidity that the immersed liquid biofilm was exposed to under those conditions. We observed that when going from no airflow to an 85% RH airflow (immediate airflow at 85% RH, as the warm-up period occurred without connection to the container) honeycomb patterns indeed formed (Fig. 4C). Similarly, going from no airflow to a 25% RH airflow also triggered honeycomb pattern formation (Fig. 4D). Taken together, these results suggest that the dissipation of a volatile compound accumulated inside the airtight container (comparable to volatile accumulation under a Petri dish lid), rather than a change in humidity, caused honeycomb-like structures to form. Therefore, we hypothesize that the immersed liquid biofilm produces a volatile compound that, when dissipated, triggers honeycomb pattern formation.

Notably, we observed that the timing of honeycomb pattern formation differs depending upon whether high- or low-humidity airflow levels were used. Going from no airflow to a high-humidity airflow caused honeycombs to form in a wide variety of time frames (one to 18 minutes), whereas going from no airflow to a low-humidity airflow caused honeycombs to form consistently within about one-and-a-half to three minutes. These results suggest that changes in humidity are not required for honeycomb pattern formation but affect the timing of the manifestation of the honeycomb patterns. This phenomenon could be explained by a faster release of medium-dissolved volatiles into low-humidity air than into high-humidity air.

Discussion

In this study, using an optimized workflow to observe the development of *H. volcanii* immersed liquid biofilms, we determined that for immersed liquid biofilm formation, this model haloarchaeon does not require any of the genes known to affect biofilm formation on abiotic surfaces. Deletion mutants lacking *pilA1-6*, which encode type IV pilins, or *pilB1C1* and *pilB3C3,* which encode proteins required for pilus assembly, all of which exhibit adhesion defects in the ALI assay, could still form immersed liquid biofilms. While the *H. volcanii* genome encodes two additional PilB and PilC paralogs and 36 additional predicted pilins (39), which can presumably form distinct type IV pili, it is unlikely that these proteins are involved in immersed liquid biofilm formation since the absence of *pibD,* which encodes the only *H. volcanii* prepilin peptidase (56) and is required to process prepilins prior to pilus assembly (58), did not affect immersed liquid biofilm formation.

Furthermore, transposon mutants affecting *H. volcanii* chemotaxis genes, which result in decreased ALI adhesion, still exhibited immersed liquid biofilm formation. However, little is known about chemotaxis and intracellular signaling of *H. volcanii*. Thus, it is possible that an alternative signaling pathway is required for the formation of immersed liquid biofilms. Similarly, immersed liquid biofilms formed independent of two major post-translational modifications of cell surface proteins, *N*-glycosylation (Δ*aglB* and Δ*agl15*) and ArtA-dependent C-terminal lipid anchoring (Δ*pssA* and Δ*pssD*). These modifications affect the function of various secreted proteins, including the S-layer glycoprotein. Nevertheless, cell surface proteins are likely to be involved in the formation of immersed liquid biofilms.

While it is intriguing that none of the genes known to affect adhesion to abiotic surfaces led to an altered immersed liquid biofilm phenotype, the process through which this type of biofilm forms remains to be elucidated. However, during this study, we also observed a previously undescribed phenomenon that could provide further insights into immersed liquid biofilms: the rapid, transient, and reproducible honeycomb pattern formation that occurs in cultures with established immersed liquid biofilms upon removal of the Petri dish lid. Chimileski et al. also noted the dynamic nature of immersed liquid biofilms, including filamentous structures extending and retracting on the edge of the Petri dish. In fact, honeycomb-like patterns might have been induced in these experiments, but a focus on longer time frames (>1 hour) and only mild disturbance of the immersed liquid biofilm headspace, by tapping or slightly lifting the lid, likely prevented the observation of honeycomb-like structures.

Since we showed here that honeycomb-like structures formed rapidly even in non-motile and non-piliated mutants, together with the short time frame of honeycomb formation, strongly suggest that this process is not driven by active movement of cells. The short time frame of honeycomb pattern formation also suggests that whatever is passively moving the cells must be present within the immersed liquid biofilm before honeycombs form. Therefore, honeycomb pattern formation may reveal the underlying structure of the immersed liquid biofilm. It has been hypothesized that the EPS components of an *H. volcanii* immersed liquid biofilm include, primarily, polysaccharides, eDNA, and amyloid proteins (45). These EPS components likely form the underlying structure providing support for the biofilm, and under the conditions tested in this study, this skeletal structure may have played a direct role in the formation of honeycomb patterns. While EPS biosynthesis pathways in *H. volcanii* remain to be characterized, the pathway of exopolysaccharide biosynthesis in *H. mediterranei* has been determined (59). Interestingly, both immersed liquid biofilm formation and honeycomb pattern formation also occurred in *H. mediterranei* (Fig. S5), suggesting that the genes required for both processes are conserved between these species.

While, to the best of our knowledge, the rapid transition from diffuse immersed liquid biofilms into honeycomb patterns has not been described so far, honeycomb-like structures have been observed in biofilms of other prokaryotes. These honeycomb patterns often appear to serve structural roles within the biofilm and form on a microscopic scale (diameters of 5 to 50 µm) over the course of hours to days (i.e. multiple generation times). For example, a honeycomb-like meshwork generated by interconnected eDNA strands bound to cells through positively charged proteins has also been reported for *Staphylococcus aureus* biofilms (60), and membrane-bound lipoproteins that can bind DNA have been implicated in maintaining the structure of *S. aureus* biofilms (61). Furthermore, in *P. aeruginosa* PAO1 biofilms, interactions between eDNA and exopolysaccharide Psl fibers result in web-like patterns observed in pellicles and flow-cells (62, 63). The web pattern might function as a supportive scaffold that allows bacterial attachment and subsequent growth within the biofilm (63). Furthermore, it might play a role in bacterial migration to facilitate nutrient uptake, since the web-like pattern is most pronounced in nutrient-starved areas within the biofilm (62). This is in line with studies in *Listeria monocytogenes* biofilms which, under conditions of constant liquid flow, form honeycomb-like ('knitted') structures in diluted, nutrient-poor media but not in rich media (64); under static conditions, honeycomb hollows were shown to contain planktonic cells, perhaps suggesting a transition to biofilm dispersal (65). A variety of benefits from honeycomb-like structures is also supported by Schaudinn *et al.*, who hypothesize that for cells undergoing stress from fluid forces, honeycombs could provide flexibility and distribution of forces over the six vertices (66). Moreover, the increased surface area of honeycombs-like structures could aid cells faced with limited nutrients and could potentially also serve as communication 'roadways' for intercellular signaling (66). Computer models of honeycomb patterns with a larger diameter (several hundred µm) observed in *Thiovulum majus* biofilms suggest that these structures cause water advection that would result in improved distribution of oxygen within the biofilm (67).

While the microscopic dimensions of these bacterial honeycomb patterns are substantially different from the macroscopic scale of the honeycomb patterns we described here for *H. volcanii* (diameters of 1 mm to 5 mm), these examples illustrate that honeycomb-like structures likely serve important biological roles. Upon honeycomb pattern formation, an upward motion (towards the ALI) of cells was observed, followed by the dissipation of the pattern (Movie S2). Since an active movement of cells is unlikely due to the lack of flagella and type IV pili in the respective mutants, which still formed honeycomb patterns, the honeycomb-like structures might contribute to increased floating properties of the biofilm. Based on the rapid formation of honeycomb patterns in *H. volcanii*, which is unparalleled in other prokaryotes, it is also tempting to speculate that this process results in turbulences in the liquid culture that could facilitate improved distribution of minerals and other nutrients from the surrounding media to the cells within the biofilm.

Based on the DPG experiments, we hypothesize that the rapid transition to honeycomb patterns was induced by the dissipation of volatiles from the headspace of the immersed liquid biofilm. Halophilic organisms have been shown to produce and release volatiles such as methanol and methanethiol (68). Acetic acid has previously been shown to act as a signal to trigger biofilm formation in *B. subtilis* (69). The ability of bacteria to use olfaction has also been explored with the discovery that airborne ammonia acts as a volatile and stimulates a response in neighboring cells (70). In general, since certain volatiles can facilitate intercellular communication (71, 72), rapid dissipation of volatile compounds might induce changes in cell physiology that results in structural changes in the biofilm such as honeycomb pattern formation. In *T. majus*, chemotaxis towards preferred oxygen concentrations results in honeycomb patterns, albeit over the course of several days (67). While we could show that *H. volcanii* honeycomb pattern formation is not dependent on oxygen, the dissipation of volatiles in the headspace above immersed liquid biofilms might still serve as an indirect signal for increased oxygen concentrations. However, other studies have questioned the importance of oxygen in regard to movement of cells within patterns, such as bioconvective pattern formations (73), indicating that other factors are at play.

Similar to the formation of immersed liquid biofilms, the molecular mechanism and genes required to form honeycomb-like structures in *H. volcanii* remain to be elucidated. However, it is worth noting that an established immersed liquid biofilm appears to be necessary for the formation of honeycomb patterns but not all immersed liquid biofilms could be triggered to form honeycomb patterns. Instead, the accumulation of volatiles seems to be an additional requirement, since experiments using a constant airflow of the DPG still led to the formation of immersed liquid biofilms, but those could not be triggered to form honeycomb-like structures. This finding further supports the hypothesis that the honeycomb pattern formation is a biological reaction to changes in the environment of the immersed liquid biofilm. Future studies focused on identifying mutants unable to form honeycombs may yield insight into: (i) the identity of the volatiles that inhibit honeycomb pattern formation; (ii) how the volatiles may benefit the biofilm and why their dispersal triggers the honeycombs; and (iii) the mechanisms through which the volatiles act, such as possible changes in gene expression, post-translational modifications, or protein stability. The volatile compound might also directly interfere with interactions between eDNA and proteins, so that its removal could stimulate the assembly of an electrostatic net and the formation of honeycomb-like structures.

In conclusion, this study showed that *H. volcanii* immersed liquid biofilms form through an as-of-yet-unknown mechanism that is independent of many of the genes required for biofilm formation at the ALI. Moreover, this study supports the notion that pattern formation within biofilms is a common phenomenon, but in contrast to previously described pattern formations in bacteria, honeycomb-like structures in *H. volcanii* can form on a macroscopic scale and within seconds, triggered by the dissipation of a volatile factor produced by the biofilm-embedded cells.

Acknowledgments

We would like to thank Fevzi Daldal, Elliot Friedman, Mark Goulian, John Hallsworth, Brent Helliker, Chinedum Osuji, and Gary Wu for helpful discussions and help with experiments. We acknowledge the Microbial Culture & Metabolomics Core of the PennCHOP Microbiome Program for assistance with culture studies. We also thank the Daldal and Helliker labs for the use of the anaerobic chamber and Dew Point Generator, respectively, as well as Ian Duggin for providing the Δ*cetZ1* strain.

S.S. was supported by the German Research Foundation (DFG Postdoctoral Fellowship, 398625447). M.P., H.S. and Z.M. were supported by the National Science Foundation Grant 1817518. C.d.V., C.R. and J.S. were supported by the Dept. of Biology Biol376 lab course fund. A.W.B.F. was supported by his personal startup fund from Brandeis University.

Conflict of interest

The authors declare no conflict of interest.

Supplemental Material

Figure S1: Immersed liquid biofilms of all analyzed mutant strains cover a similar Petri dish area and exhibit similar timing in their formation and honeycomb patterns as the wild-type. Boxplots for all

analyzed strains represent the area of a Petri dish covered by the immersed liquid biofilm (ILB) **(A)**, the time to the start of honeycomb pattern (HCP) formation after lid removal **(B)**, the time to the peak of honeycomb pattern formation after lid removal **(C)**, and the time to dispersal after peak honeycomb pattern formation. Box center line, median; box limits, upper and lower quartiles; whiskers, 1.5x interquartile range; points, all individual values. Representative images for all strains can be found in Fig. S2.

Figure S2: All tested mutant strains formed immersed liquid biofilms as well as honeycomb pattern formations. Each mutant strain (as well as the parental strains H53 and H98) was tested for **(A)** immersed liquid biofilm formation using the optimized protocol (see Fig. 1) and for **(B)** honeycomb pattern formation after opening the Petri dish lid under aerobic conditions. Images for (A) were taken within 10 seconds of Petri dish lid removal, and images for (B) were taken at peak honeycomb formation (time to reach peak honeycomb formation from lid removal noted in image). Images shown are representative for at least two replicates tested for immersed liquid biofilm and honeycomb pattern formations for each strain. The diameter of the Petri dishes is 10 cm. Quantitative analyses for all strains can be found in Fig. S1.

Figure S3: The addition of fumarate to Hv-Cab allows for growth under anaerobic conditions. (A) Different fumarate concentrations in Hv-Cab containing PIPES buffer were tested for growth under anaerobic conditions by measuring OD_{600} over six days in a 96-well plate. The anaerobic growth curves represent the mean ± SD of 16 technical replicates. **(B)** The difference in OD_{600} between the last and first time point is given as the mean ± SD for the different fumarate concentrations. Only the growth of wild-type cells in medium containing no fumarate was statistically significantly different from growth in all other fumarate concentrations ($p < 1e\text{-}15$).

Figure S4: Immersed liquid biofilm formation does not require low oxygen or high volatile accumulation. (A) After 19 hours of 80% RH airflow, an immersed liquid biofilm formed at the edges of the Petri dish. **(B)** After 19 hours of 85% RH airflow, an immersed liquid biofilm can be seen in the center and at the edges of the Petri dish. Arrows represent input airflow tubes (white) and output airflow tubes (yellow). The immersed liquid biofilm in **(A)** was observed in one of two experiments in which a constant airflow was applied for at least 19 hours. In the second experiment, the immersed liquid biofilm that formed is shown in **(B)**. The diameter of the Petri dishes is 10 cm.

Figure S5: *H. mediterranei* forms liquid biofilms and honeycomb patterns. (A) Representative images of a wild-type immersed liquid biofilm immediately after Petri dish lid removal, followed by **(B)** start of honeycomb formation 14 seconds after lid removal, **(C)** peak honeycomb pattern formation 26 seconds after lid removal, and **(D)** dispersal of the honeycomb pattern 71 seconds after lid removal, are shown. Insets are digitally magnified images (2.0x) of the indicated area. The Petri dish diameter is 10 cm.

Movie S1: *H. volcanii* form honeycomb patterns. Removal of the Petri dish lid, after an immersed liquid biofilm has formed, triggers honeycombs to form and then dissipate. Time lapse was acquired at 150 frames per second and played at actual real-time speed. Honeycomb pattern formation begins at 25 seconds and dissipation begins around 40 seconds. The Petri dish diameter is 10 cm.

Movie S2: Honeycomb pattern formations extend upwards. Honeycomb-like structures extend upwards into the liquid and appear to dissipate close to the ALI. Time lapse was acquired at 150 frames per second and played at 15x the actual speed. (Right Panel) 2.5x zoom-in projection of the delimited square on the right panel. The Petri dish diameter is 10 cm.

References

1. Flemming H-C, Wuertz S. 2019. Bacteria and archaea on Earth and their abundance in biofilms. Nat Rev Microbiol 17:247–260.
2. Kragh KN, Hutchison JB, Melaugh G, Rodesney C, Roberts AEL, Irie Y, Jensen PØ, Diggle SP, Allen RJ, Gordon V, Bjarnsholt T. 2016. Role of Multicellular Aggregates in Biofilm Formation. mBio 7:e00237-16, /mbio/7/2/e00237-16.atom.
3. Santos ALS dos, Galdino ACM, Mello TP de, Ramos L de S, Branquinha MH, Bolognese AM, Columbano Neto J, Roudbary M. 2018. What are the advantages of living in a community? A microbial biofilm perspective! Mem Inst Oswaldo Cruz 113.
4. van Wolferen M, Orell A, Albers S-V. 2018. Archaeal biofilm formation. Nat Rev Microbiol 16:699–713.
5. Høiby N, Bjarnsholt T, Givskov M, Molin S, Ciofu O. 2010. Antibiotic resistance of bacterial biofilms. Int J Antimicrob Agents 35:322–332.
6. Boudarel H, Mathias J-D, Blaysat B, Grédiac M. 2018. Towards standardized mechanical characterization of microbial biofilms: analysis and critical review. Npj Biofilms Microbiomes 4:17.
7. Shrout JD, Nerenberg R. 2012. Monitoring Bacterial Twitter: Does Quorum Sensing Determine the Behavior of Water and Wastewater Treatment Biofilms? Environ Sci Technol 46:1995–2005.
8. Edwards SJ, Kjellerup BV. 2013. Applications of biofilms in bioremediation and biotransformation of persistent organic pollutants, pharmaceuticals/personal care products, and heavy metals. Appl Microbiol Biotechnol 97:9909–9921.
9. Sanchez CJ, Mende K, Beckius ML, Akers KS, Romano DR, Wenke JC, Murray CK. 2013. Biofilm formation by clinical isolates and the implications in chronic infections. BMC Infect Dis 13:47.
10. Roberts AEL, Kragh KN, Bjarnsholt T, Diggle SP. 2015. The Limitations of In Vitro Experimentation in Understanding Biofilms and Chronic Infection. J Mol Biol 427:3646–3661.
11. Bowler PG. 2018. Antibiotic resistance and biofilm tolerance: a combined threat in the treatment of chronic infections. J Wound Care 27:273–277.
12. Olsen I. 2015. Biofilm-specific antibiotic tolerance and resistance. Eur J Clin Microbiol Infect Dis 34:877–886.
13. Hall CW, Mah T-F. 2017. Molecular mechanisms of biofilm-based antibiotic resistance and tolerance in pathogenic bacteria. FEMS Microbiol Rev 41:276–301.
14. Ceri H, Olson ME, Stremick C, Read RR, Morck D, Buret A. 1999. The Calgary Biofilm Device: New Technology for Rapid Determination of Antibiotic Susceptibilities of Bacterial Biofilms. J Clin Microbiol 37:1771–1776.
15. Li Y-H, Tian X. 2012. Quorum Sensing and Bacterial Social Interactions in Biofilms. Sensors 12:2519–2538.
16. Solano C, Echeverz M, Lasa I. 2014. Biofilm dispersion and quorum sensing. Curr Opin Microbiol 18:96–104.
17. Davies DG. 1998. The Involvement of Cell-to-Cell Signals in the Development of a Bacterial Biofilm. Science 280:295–298.
18. Davey ME, O'Toole GA. 2000. Microbial Biofilms: from Ecology to Molecular Genetics. Microbiol Mol Biol Rev 64:847–867.
19. Nadell CD, Xavier JB, Foster KR. 2009. The sociobiology of biofilms. FEMS Microbiol Rev 33:206–224.
20. Hammer BK, Bassler BL. 2003. Quorum sensing controls biofilm formation in Vibrio cholerae: Biofilms in V. cholerae. Mol

Microbiol 50:101–104.
21. Orell A, Fröls S, Albers S-V. 2013. Archaeal Biofilms: The Great Unexplored. Annu Rev Microbiol 67:337–354.
22. Conrad JC. 2012. Physics of bacterial near-surface motility using flagella and type IV pili: implications for biofilm formation. Res Microbiol 163:619–629.
23. Maier B, Wong GCL. 2015. How Bacteria Use Type IV Pili Machinery on Surfaces. Trends Microbiol 23:775–788.
24. O'Toole GA, Kolter R. 1998. Flagellar and twitching motility are necessary for *Pseudomonas aeruginosa* biofilm development. Mol Microbiol 30:295–304.
25. Klausen M, Heydorn A, Ragas P, Lambertsen L, Aaes-Jørgensen A, Molin S, Tolker-Nielsen T. 2003. Biofilm formation by Pseudomonas aeruginosa wild type, flagella and type IV pili mutants: Roles of bacterial motility in the formation of the flat P. aeruginosa biofilm. Mol Microbiol 48:1511–1524.
26. O'Toole GA, Wong GC. 2016. Sensational biofilms: surface sensing in bacteria. Curr Opin Microbiol 30:139–146.
27. Watnick PI, Fullner KJ, Kolter R. 1999. A Role for the Mannose-Sensitive Hemagglutinin in Biofilm Formation by Vibrio cholerae El Tor. J Bacteriol 181:3606–3609.
28. Pratt LA, Kolter R. 1998. Genetic analysis of *Escherichia coli* biofilm formation: roles of flagella, motility, chemotaxis and type I pili. Mol Microbiol 30:285–293.
29. Guttenplan SB, Kearns DB. 2013. Regulation of flagellar motility during biofilm formation. FEMS Microbiol Rev 37:849–871.
30. Hinsa SM, Espinosa-Urgel M, Ramos JL, O'Toole GA. 2003. Transition from reversible to irreversible attachment during biofilm formation by Pseudomonas fluorescens WCS365 requires an ABC transporter and a large secreted protein: P. fluorescens biofilm formation. Mol Microbiol 49:905–918.
31. Ivanov IE, Boyd CD, Newell PD, Schwartz ME, Turnbull L, Johnson MS, Whitchurch CB, O'Toole GA, Camesano TA. 2012. Atomic force and super-resolution microscopy support a role for LapA as a cell-surface biofilm adhesin of Pseudomonas fluorescens. Res Microbiol 163:685–691.
32. Collins AJ, Pastora AB, Smith TJ, O'Toole GA. 2020. MapA, a second large RTX adhesin conserved across the Pseudomonads, contributes to biofilm formation by *Pseudomonas fluorescens*. J Bacteriol JB.00277-20, jb;JB.00277-20v1.
33. Kobayashi K. 2007. Bacillus subtilis Pellicle Formation Proceeds through Genetically Defined Morphological Changes. J Bacteriol 189:4920–4931.
34. Yamamoto K, Arai H, Ishii M, Igarashi Y. 2012. Involvement of Flagella-Driven Motility and Pili in Pseudomonas aeruginosa Colonization at the Air-Liquid Interface. Microbes Environ 27:320–323.
35. Hölscher T, Bartels B, Lin Y-C, Gallegos-Monterrosa R, Price-Whelan A, Kolter R, Dietrich LEP, Kovács ÁT. 2015. Motility, Chemotaxis and Aerotaxis Contribute to Competitiveness during Bacterial Pellicle Biofilm Development. J Mol Biol 427:3695–3708.
36. Pohlschroder M, Esquivel RN. 2015. Archaeal type IV pili and their involvement in biofilm formation. Front Microbiol 06.
37. Chaudhury P, Quax TEF, Albers S-V. 2018. Versatile cell surface structures of archaea: Cell surface structures of archaea. Mol Microbiol 107:298–311.
38. Tripepi M, Imam S, Pohlschröder M. 2010. Haloferax volcanii Flagella Are Required for Motility but Are Not Involved in PibD-Dependent Surface Adhesion. J Bacteriol 192:3093–3102.
39. Esquivel RN, Xu R, Pohlschroder M. 2013. Novel Archaeal Adhesion Pilins with a Conserved N Terminus. J Bacteriol 195:3808–3818.
40. Esquivel RN, Pohlschroder M. 2014. A conserved type IV pilin signal peptide H-domain is critical for the post-translational regulation of flagella-dependent motility: Pili-dependent regulation of swimming motility. Mol Microbiol 93:494–504.
41. Legerme G, Pohlschroder M. 2019. Limited Cross-Complementation Between Haloferax volcanii PilB1-C1 and PilB3-C3 Paralogs. Front Microbiol 10:700.
42. Legerme G, Yang E, Esquivel R, Kiljunen S, Savilahti H, Pohlschroder M. 2016. Screening of a Haloferax volcanii Transposon Library Reveals Novel Motility and Adhesion Mutants. Life 6:41.
43. Baker BJ, Tyson GW, Webb RI, Flanagan J, Hugenholtz P, Allen EE, Banfield JF. 2006. Lineages of Acidophilic Archaea Revealed by Community Genomic Analysis. Science 314:1933–1935.
44. Justice NB, Pan C, Mueller R, Spaulding SE, Shah V, Sun CL, Yelton AP, Miller CS, Thomas BC, Shah M, VerBerkmoes N, Hettich R, Banfield JF. 2012. Heterotrophic Archaea Contribute to Carbon Cycling in Low-pH, Suboxic Biofilm Communities. Appl Environ Microbiol 78:8321–8330.
45. Chimileski S, Franklin MJ, Papke RT. 2014. Biofilms formed by the archaeon Haloferax volcaniiexhibit cellular differentiation and social motility, and facilitate horizontal gene transfer. BMC Biol 12:65.
46. de Silva RT, Abdul-Halim MF, Pittrich DA, Brown HJ, Pohlschroder M, Duggin IG. 2020. Improved growth and morphological plasticity of *Haloferax volcanii*. preprint, Microbiology.
47. Dyall-Smith M. 2009. The Halohandbook: protocols for halobacterial genetics v.7.3.
48. Allers T, Ngo H-P, Mevarech M, Lloyd RG. 2004. Development of Additional Selectable Markers for the Halophilic Archaeon Haloferax volcanii Based on the leuB and trpA Genes. Appl Environ Microbiol 70:943–953.
49. Tripepi M, Esquivel RN, Wirth R, Pohlschröder M. 2013. Haloferax volcanii cells lacking the flagellin FlgA2 are hypermotile. Microbiology 159:2249–2258.
50. Abu-Qarn M, Eichler J. 2006. Protein N-glycosylation in Archaea: defining Haloferax volcanii genes involved in S-layer glycoprotein glycosylation. Mol Microbiol 15.
51. Kaminski L, Guan Z, Yurist-Doutsch S, Eichler J. 2013. Two Distinct N-Glycosylation Pathways Process the Haloferax volcanii S-Layer Glycoprotein upon Changes in Environmental Salinity. mBio 4:e00716-13, mBio.00716-13.
52. Abdul-Halim MF, Schulze S, DiLucido A, Pfeiffer F, Filho AWB, Pohlschroder M. 2020. Lipid Anchoring of Archaeosortase Substrates and Midcell Growth in Haloarchaea 11:14.
53. Duggin IG, Aylett CHS, Walsh JC, Michie KA, Wang Q, Turnbull L, Dawson EM, Harry EJ, Whitchurch CB, Amos LA, Löwe J. 2015. CetZ tubulin-like proteins control archaeal cell shape. Nature 519:362–365.
54. Schindelin J, Arganda-Carreras I, Frise E, Kaynig V, Longair M, Pietzsch T, Preibisch S, Rueden C, Saalfeld S, Schmid B, Tinevez J-Y, White DJ, Hartenstein V, Eliceiri K, Tomancak P, Cardona A. 2012. Fiji: an open-source platform for biological-image analysis. Nat Methods 9:676–682.
55. Oren A. 1991. Anaerobic growth of halophilic archaeobacteria by reduction of fumarate. J Gen Microbiol 137:1387–1390.
56. Hartman AL, Norais C, Badger JH, Delmas S, Haldenby S, Madupu R, Robinson J, Khouri H, Ren Q, Lowe TM, Maupin-Furlow J, Pohlschroder M, Daniels C, Pfeiffer F, Allers T, Eisen JA. 2010. The Complete Genome Sequence of Haloferax volcanii DS2, a Model Archaeon. PLoS ONE 5:e9605.

57. Esquivel RN, Schulze S, Xu R, Hippler M, Pohlschroder M. 2016. Identification of *Haloferax volcanii* Pilin *N* -Glycans with Diverse Roles in Pilus Biosynthesis, Adhesion, and Microcolony Formation. J Biol Chem 291:10602–10614.
58. Tripepi M, You J, Temel S, Önder Ö, Brisson D, Pohlschröder M. 2012. N-Glycosylation of Haloferax volcanii Flagellins Requires Known Agl Proteins and Is Essential for Biosynthesis of Stable Flagella. J Bacteriol 194:4876–4887.
59. Zhao D, Cai L, Wu J, Li M, Liu H, Han J, Zhou J, Xiang H. 2013. Improving polyhydroxyalkanoate production by knocking out the genes involved in exopolysaccharide biosynthesis in Haloferax mediterranei. Appl Microbiol Biotechnol 97:3027–3036.
60. Warraich AA, Mohammed AR, Perrie Y, Hussain M, Gibson H, Rahman A. 2020. Evaluation of anti-biofilm activity of acidic amino acids and synergy with ciprofloxacin on Staphylococcus aureus biofilms. Sci Rep 10:9021.
61. Kavanaugh JS, Flack CE, Lister J, Ricker EB, Ibberson CB, Jenul C, Moormeier DE, Delmain EA, Bayles KW, Horswill AR. 2019. Identification of Extracellular DNA-Binding Proteins in the Biofilm Matrix. mBio 10:e01137-19, /mbio/10/3/mBio.01137-19.atom.
62. Wang S, Parsek MR, Wozniak DJ, Ma LZ. 2013. A spider web strategy of type IV pili-mediated migration to build a fibre-like Psl polysaccharide matrix in *Pseudomonas aeruginosa* biofilms: Type IV pili build a Psl-fibre biofilm matrix. Environ Microbiol 15:2238–2253.
63. Wang S, Liu X, Liu H, Zhang L, Guo Y, Yu S, Wozniak DJ, Ma LZ. 2015. The exopolysaccharide Psl-eDNA interaction enables the formation of a biofilm skeleton in *P seudomonas aeruginosa*: Psl-eDNA interaction and biofilm skeleton. Environ Microbiol Rep 7:330–340.
64. Cherifi T, Jacques M, Quessy S, Fravalo P. 2017. Impact of Nutrient Restriction on the Structure of Listeria monocytogenes Biofilm Grown in a Microfluidic System. Front Microbiol 8:864.
65. Guilbaud M, Piveteau P, Desvaux M, Brisse S, Briandet R. 2015. Exploring the Diversity of Listeria monocytogenes Biofilm Architecture by High-Throughput Confocal Laser Scanning Microscopy and the Predominance of the Honeycomb-Like Morphotype. Appl Environ Microbiol 81:1813–1819.
66. Schaudinn C, Costerton B, Stoodley P, Robinson D, Webster P, Baum M, Ehrlich G, Kainović A, Teresa O. 2007. Bacterial Biofilms, Other Structures Seen as Mainstream Concepts. Microbe Mag 2:231–237.
67. Thar R, Kühl M. 2005. Complex pattern formation of marine gradient bacteria explained by a simple computer model. FEMS Microbiol Lett 246:75–79.
68. Nordmann B, Lebert MR, Alam M, Nitz S, Kollmannsberger H, O-esterhelt D, Hazelbauer GL. 1994. Identification of volatile forms of methyl groups released by Halobacterium salinarium. J Biol Chem 269:16449–16454.
69. Chen Y, Gozzi K, Yan F, Chai Y. 2015. Acetic Acid Acts as a Volatile Signal To Stimulate Bacterial Biofilm Formation. mBio 6:e00392-15.
70. Nijland R, Burgess JG. 2010. Bacterial olfaction. Biotechnol J 5:974–977.
71. Audrain B, Farag MA, Ryu C-M, Ghigo J-M. 2015. Role of bacterial volatile compounds in bacterial biology. FEMS Microbiol Rev 39:222–233.
72. Serasanambati M, Broza YY, Haick H. 2019. Volatile Compounds Are Involved in Cellular Crosstalk and Upregulation. Adv Biosyst 3:1900131.
73. Janosi IM, Czirok A, Silhavy D, Holczinger A. 2002. Is bioconvection enhancing bacterial growth in quiescent environments? Environ Microbiol 4:525–531.